Single magnetic particle dynamics in a microchannel

Ashok Sinha, Ranjan Ganguly, Anindya K. De, and Ishwar K. Puri

Citation: Physics of Fluids (1994-present) **19**, 117102 (2007); doi: 10.1063/1.2780191
View online: http://dx.doi.org/10.1063/1.2780191
View Table of Contents: http://scitation.aip.org/content/aip/journal/pof2/19/11?ver=pdfcov
Published by the AIP Publishing

PHYSICS OF FLUIDS **19**, 117102 (2007)

Single magnetic particle dynamics in a microchannel

Ashok Sinha
Department of Engineering Science and Mechanics, Virginia Polytechnic Institute and State University, Blacksburg, Virginia 24061, USA

Ranjan Ganguly
Department of Power Engineering, Jadavpur University, Kolkata 700032, India

Anindya K. De and Ishwar K. Puri[a)]
Department of Engineering Science and Mechanics, Virginia Polytechnic Institute and State University, Blacksburg, Virginia 24061, USA

(Received 10 May 2007; accepted 14 August 2007; published online 7 November 2007)

Functionalized magnetic particles are used in micrototal analysis systems since they act as magnetically steered mobile substrates in microfluidic channels, and can be collected for bioanalytical processing. Here, we examine the motion of magnetic microbeads in a microfluidic flow under the influence of a nonuniform external magnetic field and characterize their collection in terms of the magnetic field strength, particle size, magnetic susceptibility, host fluid velocity and viscosity, and the characteristic length scale. We show that the collection efficiency of a magnetic collector depends upon two dimensionless numbers that compare the magnetic and particle drag forces. © *2007 American Institute of Physics*. [DOI: 10.1063/1.2780191]

Magnetic microspheres consist of suspensions of superparamagnetic[1] ferrite nanoparticles of ~10 nm in diameter that are embedded within nonmagnetic 1–2 μm diameter polymer spheres. These microspheres can be attached to various bioanalytes or cells with high selectivity by functionalizing the bead surfaces with suitable bioconjugates, making it possible to manipulate the analyte-bead amalgam with external magnetic fields.[2–4] Magnetic microspheres have been used in microfluidic micro-total-analytical-systems devices, which are tools for biological and biochemical analyses.[5] These beads are easily recovered by using high gradient magnetic separation.[6] Externally manipulated magnetic microspheres provide high surface-to-volume ratio mobile surfaces for chemical[7] and biochemical reactions,[8] and have been used in microfluidic devices.[9] Recent advances in photolithography allow the production of magnetic gradients exceeding 10^5 T/m in microelectromechanical systems (MEMS) devices,[10] enabling the manipulation of isolated magnetic microspheres in a controlled fashion. Functionalized walls or magnetic microspheres can be used for protein microarrays;[11] DNA purification;[12] DNA sequencing and separation;[13] *in vitro* cell manipulation and separation;[14] and *in vivo* drug targeting.[15] The predominant transport issue here is the precise magnetic manipulation of microbeads in a microfluidic flow.

Experimental investigations have so far only provided qualitative demonstrations of how microfabricated electromagnets can generate a strong enough force field to ensure particle capture[16,17] or separation,[18] or enable MEMS-based cell sorters.[19] While useful, these investigations do not provide a quantitative particle-tracking model that is applicable regardless of configuration and geometry. Previous simulations of magnetic particle transport in microfluidic contexts[20] have also not focused on individual particle trajectories or detailed parametric analyses. Mikkelsen and Bruus[21] offered a theoretical analysis on the microfluidic transport and capture of 1 μm diameter magnetic microspheres. Their continuum approach including the particles is questionable, since in water such a treatment is generally valid only for Fe_3O_4 particles diameters smaller than 40 nm.[22] Limited parametric investigations on particle transport in the context of microfluidics and magnetic drug targeting have also been conducted by other groups[15,23,24] but such studies have not identified the key nondimensional parameters that influence magnetophoretic particle capture in different but geometrically similar systems.

Herein, we obtain attain unambiguous information about the motion of isolated particles in a microchannel flow. We use an external magnetic field to direct and steer the particles across the microchannel. Numerical simulations are performed to predict particle collection, and are validated through experiments. Next, parametric simulations illustrate the effects of flow and magnetic parameters on the particle collection efficiency in the microchannel. Our investigation concerns both the transport of an isolated particle or of very dilute suspensions for which the dipole-dipole interaction among adjacent particles is negligible.

The experiments follow the motion of magnetic microspheres suspended in a distilled water flow within a microchannel. A pressure-driven flow is established in borosilicate capillary tubes of rectangular (100 μm $\times$ 2000 μm) cross section and 100 mm length by maintaining a fixed level difference between the reservoirs at the ends of the channel. (A 7 mm height difference institutes a peak centerline velocity of 1 mm/s.) The host water flow is laden with a very dilute concentration of 1 μm diameter magnetic polystyrene microspheres (PMSi-H1.0-5 Kisker-Biotech). The magnetic par-

[a)]Author to whom correspondence should be addressed. Telephone: +1 540-231-3243. Fax: +1 540-231-4574. Electronic mail: ikpuri@vt.edu

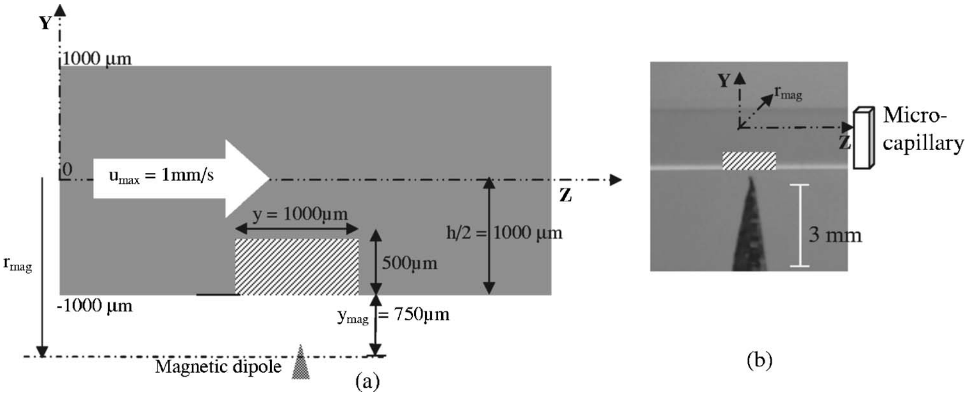

FIG. 1. (a) Schematic diagram (not to scale) of the domain. The hatched section represents the experimental viewing window. The bottom offset includes the channel thickness and displacement of the outer channel edge from the electromagnet tip. (b) Image of capillary and electromagnet during the experiments. The hatched region corresponds to that in (a).

ticles are steered by applying a nonuniform magnetic field that is established by an electromagnet with a tapered tip (that approximates a point dipole) and an adjustable current coil. A schematic diagram of the experimental configuration is presented in Fig. 1. The magnetic field distribution is made using a gaussmeter. Since the microfluidic channel has a dimension comparable to the spatial resolution of the gaussmeter probe (~1 mm), the field distribution inside the channel could not be evaluated directly from its readings. Instead, magnetic field measurements are made over a larger 5 mm $\times$5 mm domain and the local field strength and gradient at the channel location are subsequently obtained through interpolation. The measured field strength is 1300 G at $y=0$, and rapidly diminishes to 300 G at the top of the 500 μm wide region of interest. The strength and distance of an equivalent point dipole used in the numerical simulations is so chosen that its field and gradient at the channel midplane match the corresponding measured values. Although the electromagnet used in the experiment has a finite size, the point dipole assumption accurately predicts the experimentally established field in the region close to the tip when the dipole offset distance y_{mag} (see Fig. 1) and strength are suitably adjusted. Direct images are obtained using a digital zoom microscope coupled with an additional objective lens at 100$\times$ magnification.

The transport of magnetic microspheres in microfluidic channels is influenced by both hydrodynamic and the magnetic forces. We neglect dipole-dipole interactions between neighboring particles, which is appropriate for dilute particle suspensions. The Brownian force is generally negligible for larger particles.[22] The model considers one-way coupling between the fluid and the particles in the dilute suspension; i.e., only the particle trajectory is influenced by drag due to the fluid and not *vice versa*.

A point dipole of strength m is used to represent the magnetic field $\vec{H}=-\vec{m}/|\vec{r}'|^3+3(\vec{m}\cdot\vec{r}')\vec{r}'/|\vec{r}'|^5$, where the position vector $\vec{r}'$ is measured from the dipole. Here, the dipole aligned along the y direction ($\vec{m}=\mathrm{m}\hat{j}$) is placed at a location y_{mag} below the channel. This location corresponds to the position of the tapered magnetic tip in the experiments. We assume a fully developed pressure-driven flow that has a gradient $-dp/dx=G$ through the rectangular channel that has a height h and a width b. The fluid velocity[25]

$$\vec{V}_l(x,y)=\left(\frac{Gh^2}{8\eta}\right)\frac{32}{\pi^3}\sum_{n=0}^{\infty}\left(\frac{(-1)^n}{(2n+1)^3}\right)\times\left\{1-\frac{\cosh\left[\frac{(2n+1)\pi x}{h}\right]}{\cosh\left[\frac{(2n+1)\pi b}{2h}\right]}\right\}\times\cos\left[\frac{(2n+1)\pi y}{h}\right]\hat{k}. \tag{1}$$

For the experimental capillary tube aspect ratio of 1:200, the velocity profile is nearly parabolic in the x direction and exhibits an approximately top-hat profile in the cross-stream y direction. The Newtonian relation for particle motion in terms of its absolute velocity $\vec{V}_p$, $(\frac{4}{3}\pi a^3\rho_p)d\vec{V}_p/dt=[\vec{F}_m+\vec{F}_d+\vec{F}_g]$, the right-hand side of which contains the magnetic, drag, and gravity-induced forces; i.e.,

$$\vec{F}_m=\mu_0\left(\frac{4}{3}\pi a^3\right)\left[\chi_i\bigg/\left(1+\frac{1}{3}\chi_i\right)\right]\frac{1}{2}\nabla(\vec{H}_0\cdot\vec{H}_0),$$
$$\vec{F}_d=6\pi a\eta(\vec{V}_l-\vec{V}_p),\quad \vec{F}_g=\left(\frac{4}{3}\pi a^3\right)(\rho_p-\rho_l)\vec{g}. \tag{2}$$

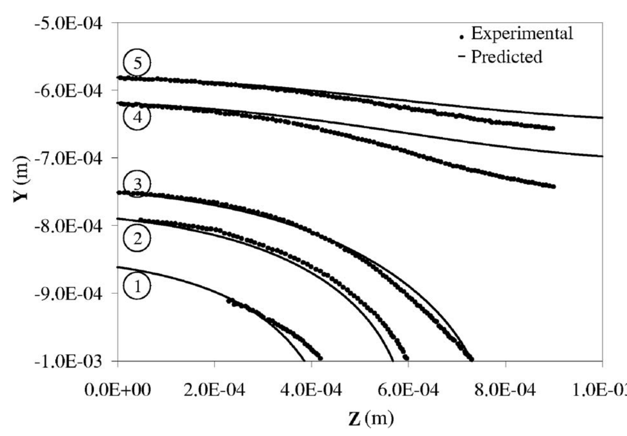

FIG. 2. Particle trajectories. Here, $U=1$ mm/s, $m=2.28\times10^{-7}$ A m^2, $a=1\times10^{-6}$ m, $\chi=0.1$, $\eta=0.000\,89$ Pa s, and $r_{\text{mag}}=1.75\times10^{-3}$ m.

For a 1 μm diameter microsphere, the particle drag force $\approx$8.4 pN with a fluid viscosity of 0.000 89 Pa S and a relative particle velocity of 1 mm/s. The gravitational force $\approx$0.004 pN (assuming $\rho_p = 1800\ \mathrm{kg/m^3}$ and $\rho_l = 1000\ \mathrm{kg/m^3}$) is negligible in comparison. The particle inertia force can be likewise neglected for the small particle mass ($\sim$0.94 pg) unless the particle acceleration exceeds an improbably large value ($\sim 1000\ \mathrm{m/s^2}$). The particle drag force thus balances the magnetic force,[22] i.e., $\vec{F}_m = -\vec{F}_d$, and $\vec{V}_p = 1/6\pi\eta a\vec{F}_m + \vec{V}_l(x,y)$, with

$$\vec{F}_{\mathrm{m}} = -4m^2\mu_o\chi_{\mathrm{eff}}\pi a^3\left\{\frac{x'(x'^2+5y'^2+z'^2)\hat{i}+4y'^3\hat{j}+z'(x'^2+5y'^2+z'^2)\hat{k}}{(x'^2+y'^2+z'^2)^5}\right\}, \tag{3}$$

where (x',y',z') denotes the coordinates with respect to the origin of the dipole [located at $(x_{\mathrm{mag}}, -y_{\mathrm{mag}}, z_{\mathrm{mag}})$] and $\chi_{\mathrm{eff}} = [\chi_i/(1+\frac{1}{3}\chi_i)]$ denotes the effective susceptibility of the spherical particles. From Eq. (3), the particle position at any instant is $\vec{r}(t) = \int_0^t \vec{V}_p(t)\mathrm{d}t + \vec{r}_o$, which we solve for using a forward differencing time-marching scheme. For solution stability, the differencing time interval δt is chosen such that the particle does not travel more than 1/1000 of the channel height in one time step; i.e., $(|\vec{V}_p| \times dt \leq 0.1\ \mu\mathrm{m})$.

Figure 2 presents a comparison between predictions and measurements for particles released from the inlet at five separate positions. The simulations consider particles of 1 μm size, particle magnetic susceptibility of 0.1, fluid viscosity of 0.000 89 Pa s, and average fluid velocity of 1 mm/s through the channel. The corresponding pairs of measured and simulated trajectories are numbered 1 through 5. The measured trajectories show that the optimal combination of modeled values of m and the magnet displacement from the channel centerline r_{mag} are $2.28\times10^{-7}\ \mathrm{A\ m^2}$ and 1.75×10^{-4} m, respectively. For all cases, the predictions and measurements are in generally good agreement, although there are small local deviations, since the model of the magnetic field is an idealization while, due to its greater complexity, the experimentally established field cannot be adequately described through a simple analytic relation. Predictions of the field gradient experienced by particles that lie closer to the magnet slightly exceed their experimentally established values. Hence, the simulated trajectories 1 and 2 fall somewhat short of their measured particle capture locations. The simulated point dipole accurately predicts the actual field gradients experienced along trajectory 3 and thus capture location. Similarly, the gradient predictions are slightly larger along trajectories 4 and 5 that are relatively further removed from the dipole origin.

Having validated the simulations, we next characterize the important parameters that influence the particle trajectories. It is intuitive that χ_{eff}, m, a, U, η, and a characteristic length scale L all have an effect, since these are all implicitly contained in the equation of motion. The capture of magnetic particles can be quantified through a capture efficiency $\Phi \propto f(\chi_{\mathrm{eff}}^{\alpha} m^{\beta} a^{\gamma} U^{\delta} \eta^{\lambda} L^{\kappa})$. It represents the ratio of the number of particles retained in the channel compared with the total number introduced into the microchannel in case of a steady flow of a homogeneous magnetic microsphere suspension. An alternate description is obtained by identifying the marginally collected particle trajectory. Particles below this trajectory are collected but those above it escape the collector; hence, $\Phi = y_0/h$. Thus, information about the initial position y_0 of the marginally collected particle at the inlet plane $z=0$ is sufficient to predict the (0,1) collection possibility for any particle above or below this position.

The normalized magnetophoretic velocity term is a function of the dimensionless ratio of the magnetic to the particle drag force; namely,

$$\Pi_1 = \frac{F_m}{F_d} \propto \frac{a^2\mu_o m^2\chi}{\eta U L^7} = \frac{[\mathrm{m}]^2[\mathrm{N/A^2}][\mathrm{A\ m^2}]^2[1]}{[\mathrm{Ns/m^2}][\mathrm{m/s}][\mathrm{m}]^7}. \tag{4}$$

An increase in the magnetic susceptibility and the magnet dipole strength increase the magnetic body force acting on a particle. For a specified particle magnetic susceptibility, both the particle magnetization and the local field gradient scale according to m, which then bears a second-order relationship with Π_1. The magnetic force depends upon the particle volume $\sim a^3$, while the drag force is proportional to the particle radius a; i.e., the ratio of the two forces depends on a^2. The particle drag force is proportional to η and to the particle relative velocity. The magnetic field strength and its gradient, and thus the magnetic force, decrease with increasing displacement of the particle from the dipole.

The axial viscous drag force on a particle competes with the cross-stream magnetic force by resisting magnetophoretic particle motion and sweeping the particles downstream. Therefore, the capture efficiency also intuitively depends on the ratio Π_1 of these two forces. This hypothesis is corroborated in Fig. 3(a) in which all the data collapse on a single curve. One would intuitively expect a linear relationship between Φ and Π_1 in a homogeneous velocity field that experiences a constant magnetic field gradient. However, both the magnetic field and fluid velocity distributions are spatially nonlinear in our case so that the Φ versus Π_1 data in Fig. 3(a) require a nonlinear fit with differing exponents for the different regions discussed previously. While there are several curve-fit options, the one we present provides two piecewise linear (on a logarithmic scale) curves that follow the correlations:

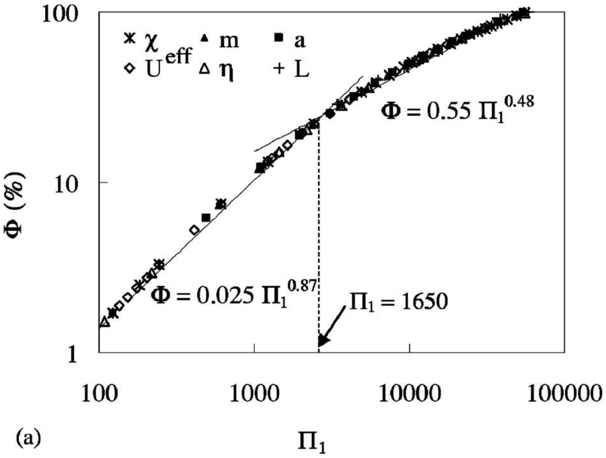

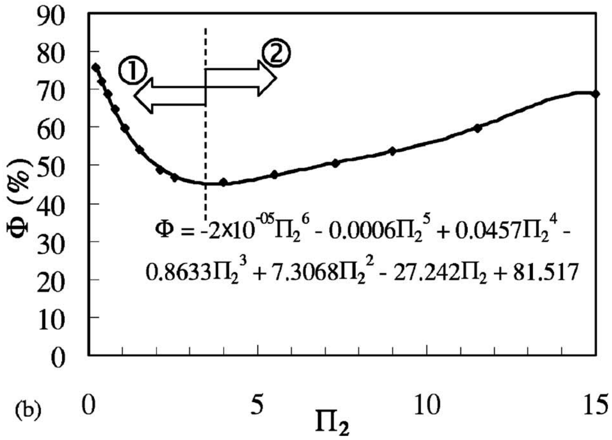

FIG. 3. (a) Variation of Φ with Π_1 for constant values of $\Pi_2=2y_{\mathrm{mag}}/h$ (=0.75). (b) Variation of Φ with respect to Π_2 for a specified value of Π_1 (=12 250). Region ① shows that increasing values of y_{mag} has a strong influence on Φ. In contrast, in region ②, the diminishing values of h have a strong influence on Φ.

$$\Phi = 0.025\Pi_1^{0.87} \quad \text{for } \Pi_1 < 1650 \text{ and}$$
$$\Phi = 0.55\Pi_1^{0.48} \quad \text{for } \Pi_1 > 1650. \tag{5}$$

Here, for $\Pi_1 < 1650$, $\alpha=0.87$, $\beta=\gamma=1.74$, $\delta=\lambda=-0.87$, and $\kappa=-6.09$, while $\alpha=0.48$, $\beta=\gamma=0.96$, $\delta=\lambda=-0.48$, and $\kappa=-3.36$ for $\Pi_1 > 1650$. A larger Π_1 value represents a stronger magnetic force that results in a high particle capture. Use of Fig. 3 enables the selection of Π_1 for a desired value of Φ in a microfluidic application.

In Fig. 3(b) and Eq. (4), the value of L is selected as the distance of the channel centerline from the dipole origin; i.e., $L=r_{\mathrm{mag}}$ (see Fig. 1). However, $r_{\mathrm{mag}}=y_{\mathrm{mag}}+h/2$; i.e., it depends on the channel half-height ($h/2$) and the distance of the magnet from the lower wall y_{mag}. The data in Fig. 3(a) represent variation of Φ with Π_1 for fixed Π_2 ($=2y_{\mathrm{mag}}/h$) accomplished by appropriately varying y_{mag} and h. In a family of geometrically similar channels having different physical dimensions, magnetic and hydrodynamic similarities require that the ratio $2y_{\mathrm{mag}}/h$ remain constant irrespective of the values of y_{mag} and h. Thus, for a given value of Π_2, the local distributions of F_m/F_d inside the channel are similar for all values of Π_1. This collapses all the data for various parametric values on a single curve. However, if Π_2 is also varied, the data fall on distinct curves, each corresponding to a specified Π_2 value.

The nonlinear dependence of Φ with Π_2 while maintaining Π_1 constant is illustrated in Fig. 3(b). Here, y_{mag} and h are varied, but all other parameters are held unchanged. The figure shows that the capture efficiency initially decreases and then increases as Π_2 increases. The minima of the curve corresponds to a minimum capture efficiency $\Phi=45\%$ for $\Pi_2=4.0$. If the value of L is held constant, an increase in Π_2 occurs when y_{mag} increases in value while that of h decreases. The data in Fig. 3(b) are divided into two regions corresponding to small and large Π_2. For small Π_2, the values of h are large, while those of y_{mag} are relatively small (in the region labeled ① in the figure). Here, a small increase in y_{mag} has a pronounced effect on the location of the critically captured particle (i.e., y_0 decreases more rapidly than does h). This explains the observed decrease in the value of Φ. For $\Pi_2 > 4.0$, i.e., for relatively larger y_{mag} values and hence small h values [region ② in Fig. 3(b)], changes in y_{mag} have a smaller influence on Φ than in region ①. Since the denominator in the capture efficiency expression decreases more rapidly than does the numerator, the capture efficiency with increasing y_{mag} again increases in region ②. Figure 3(b) also provides a basis to design to microfluidic separation devices that utilize magnetic microsphere separation.

For various combinations of the operating parameters applied to a specified geometry, the capture efficiency depends solely on Π_1 that characterizes the ratio of the magnetic and viscous drag forces on the particles. If the geometry is altered, the values of Φ in various channels depend on Π_2, which is the ratio of the distance of the magnet from the channel to the channel height. These correlations provide a method to rationally design magnetic particle separators over a wide range of operating conditions.

We dedicate this paper to Professors Kevin Granata and Liviu Librescu who were tragically killed on April 16, 2007 at Virginia Tech while answering a call to serve discovery and education.

[1]B. M. Berkovsky, *Proceedings of the International Advanced Course and Workshop on Thermomechanics of Magnetic Fluids* (Hemisphere, Washington, DC, 1978). p. 149.

[2]A. Radbruch, B. Mechtold, A. Thiel, S. Miltenyi, and E. Pfluger, "High-gradient magnetic cell sorting," Methods Cell Biol. **42**, 387 (1994).

[3]J. Ugelstad, P. Stenstad, L. Kilaas, W. S. Prestvik, R. Herje, A. Berge, and E. Hornes, "Monodisperse magnetic polymer particles—new biochemical and biomedical applications," Blood Purif **11**, 349 (1993).

[4]R. Ganguly and I. K. Puri, "Field-assisted self-assembly of superparamagnetic nanoparticles for biomedical, MEMS and BioMEMS applications," Adv. Appl. Mech. **41**, 293 (2007).

[5]M. Dufva and C. B. V. Christensen, "Diagnostic and analytical applications of protein microarrays," Expert Rev. Proteomics **2**, 41 (2005).

[6]T. Ohara, H. Kumakura, and H. Wada, "Magnetic separation using superconducting magnets," Physica C **357–360**, 1272 (2001).

[7]G. H. Seong and R. M. Crooks, "Efficient mixing and reactions within microfluidic channels using microbead-supported catalysts," J. Am. Chem. Soc. **124**, 13360 (2002).

[8]H. Chou, C. Spence, A. Scherer, and S. R. Quake, "A microfabricated device for sizing and sorting DNA molecules," Proc. Natl. Acad. Sci. U.S.A. **96**, 11 (1999).

[9]C. Pichot, "Surface-functionalized latexes for biotechnological applications," Curr. Opin. Colloid Interface Sci. **9**, 213 (2004).

[10]C. S. Lee, H. Lee, and R. M. Westervelt, "Microelectromagnets for the control of magnetic nanoparticles," Appl. Phys. Lett. **79**, 3308 (2001).
[11]V. N. Morozov and T. Y. Morozova, "Active bead-linked immunoassay on protein microarrays," Anal. Chim. Acta **564**, 40 (2006).
[12]M. Park and J. Chang, "High throughput human DNA purification with aminosilanes tailored silica-coated magnetic nanoparticles," Mater. Sci. Eng., C **27**, 1232 (2007).
[13]P. S. Doyle, J. Bibette, A. Bancaud, and J-L. Viovy, "Self-assembled magnetic matrices for DNA separation chips," Science **295**, 2237 (2002).
[14]H. Suzuki, C-M. Ho, and N. Kasagi, "A chaotic mixer for magnetic bead-based micro cell sorter," J. Microelectromech. Syst. **13**, 779 (2004).
[15]Gh. Iacob, O. Rotariub, N. J. C. Strachan, and U. O. Häfeli, "Magnetizable needles and wires—modeling an efficient way to target magnetic microspheres *in vivo*," Biorheology **41**, 599 (2004).
[16]K. Smistrup, B. G. Kjeldsen, J. L. Reimers, M. Dufva, J. Peterson, and M. F. Hansen, "On-chip magnetic bead microarray using hydrodynamic focusing in a passive magnetic separator," Lab Chip **5**, 1315 (2005).
[17]A. Rida and M. A. M. Gijs, "Dynamics of magnetically retained supraparticle structures in a liquid flow," Appl. Phys. Lett. **85**, 4986 (2004).
[18]B. B. Yellen and G. Friedman, "Programmable assembly of colloidal particles using magnetic micro-well templates," Langmuir **20**, 2553 (2004).
[19]Z. Jiang, J. Llandro, T. Mitrelias, and J. A. C. Bland, "An integrated microfluidic cell for detection, manipulation, and sorting of single micron-sized magnetic beads," J. Appl. Phys. **99**, 08S105 (2006).
[20]K. Smistrup, O. Hansen, H. Bruus, and M. F. Hansen, "Magnetic separation in microfluidic systems using microfabricated electromagnets—experiments and simulations," J. Magn. Magn. Mater. **293**, 597 (2005).
[21]C. Mikkelsen and H. Bruus, "Microfluidic capturing-dynamics of paramagnetic bead suspensions," Lab Chip **5**, 1293 (2005).
[22]E. P. Furlani, "Analysis of particle transport in a magnetophoretic microsystem," J. Appl. Phys. **99**, 024912 (2006).
[23]E. P. Furlani, "Magnetophoretic separation of blood cells at the microscale," J. Phys. D **40**, 1313 (2006).
[24]E. P. Furlani and K. C. Ng, "Analytical model of magnetic nanoparticle transport and capture in the microvasculature," Phys. Rev. E **73**, 061919 (2006).
[25]N. Ichikawa, K. Hosokawa, and R. Maeda, "Interface motion of capillary-driven flow in rectangular microchannel," J. Colloid Interface Sci. **280**, 155 (2004).